Atmos. Chem. Phys. Discuss., doi:10.5194/acp-2016-1088, 2017
Manuscript under review for journal Atmos. Chem. Phys.
Published: 13 January 2017

Atmospheric Chemistry and Physics Discussions

Intraseasonal to interannual variability of Kelvin wave momentum fluxes as derived from high-resolution radiosonde data

Jeremiah P. Sjoberg[1,2], Thomas Birner[1], and Richard H. Johnson[1]

[1]Department of Atmospheric Science, Colorado State University, Fort Collins, CO 80521
[2]now at: COSMIC Project Office, University Corporation for Atmospheric Research, Boulder, Colorado

Correspondence to: Jeremiah P. Sjoberg (sjoberg@ucar.edu)

Abstract. Observational estimates of Kelvin wave momentum fluxes in the tropical lower stratosphere remains challenging. Here we extend a method based on linear wave theory to estimate time series of these momentum fluxes from high-resolution radiosonde data. Testing the sensitivity to vertical resolution, our estimated momentum fluxes are found to be most sensitive to vertical resolution greater than 1 km, largely due to overestimation of the vertical wavelength. Estimates of momentum fluxes derived from reanalyses and coarse-resolution satellite data are notably larger. Daily time series are produced for sounding sites operated by the U.S. Department of Energy (DOE) and from the recent Dynamics of the Madden-Julian Oscillation (DYNAMO) field campaign. Our momentum flux estimates are found to be robust to different data sources and processing, and in quantitative agreement with estimates from prior studies. Climatological analysis is performed over the selected 11 year span of data from the ARM sites. Analyses for the available 11-year span of data reveal the expected seasonal cycle of momentum flux maxima in boreal winter and minima in boreal summer and variability associated with the quasi-biennial oscillation (QBO) of maxima during easterly phase and minima during westerly phase. Analysis of Madden-Julian Oscillation (MJO) active periods suggests that the MJO provides a nontrivial increase in lowermost stratospheric momentum fluxes, though statistical significance is not found due to the small number of events observed in the available time series.

1 Introduction

Atmospheric equatorial Kelvin waves represent a tropical eastward propagating wave disturbance generated primarily by convection. As tropical convection is nearly ubiquitous, particularly near to the Intertropical Convergence Zone, Kelvin waves are regular phenomena. These equatorially trapped waves have zero meridional wind perturbations and are a consequence of the equatorial beta-effect (Gill, 1982). Convectively coupled Kelvin waves are important for tropospheric phenomena, such as the Madden-Julian Oscillation (MJO) and the El Nino Southern Oscillation (ENSO) (Straub et al., 2006; Kiladis et al., 2009). These interactions arise from the eastward emanation of energy associated with these waves. Energy is also emitted upwards by Kelvin waves into the tropical tropopause layer (TTL). In particular, these waves transport westerly momentum from the troposphere into the TTL and above.

Due to this upward flux of westerly momentum, Kelvin waves are known to influence the downward progression of stratospheric westerlies that occur during a roughly 28 month cycle of winds known as the Quasi-Bienniel oscillation (QBO). There

Atmos. Chem. Phys. Discuss., doi:10.5194/acp-2016-1088, 2017
Manuscript under review for journal Atmos. Chem. Phys.
Published: 13 January 2017

Atmospheric Chemistry and Physics Discussions

is an established connection between the QBO and midwinter polar stratospheric variability (Garfinkel et al., 2012), large-scale extratropical weather patterns (Thompson et al., 2002), and ozone chemistry (Randel and Wu, 1996). Prior studies have shown that the QBO affects the vertical extent of convection (Collimore et al., 2003) and, through modulation of the cold-point temperature, affects stratospheric water vapor (Fueglistaler and Haynes, 2005).

Phasing of the QBO is initiated in the upper stratosphere by gravity waves of identical propagation direction to that of the winds (e.g. for westerly winds, westward-propagating gravity waves drive reversal to easterlies; Baldwin et al., 2001). In the middle to lowermost stratosphere, additional waves come into play in each phase: Rossby waves and mixed Rossby-gravity waves during westerly phases and Kelvin waves during easterly phases. The various wave modes propagate upwards until they reach a critical level (i.e. where the background wind matches the phase speed of a given wave) and dissipate, depositing the transported momentum. The oscillation of the QBO is a manifestation of this wave-mean flow interaction. For a given state of the zonal winds (e.g. easterly), waves with phase speed in the direction of the mean flow (e.g. Rossby waves) encounter a critical level in the lower stratosphere and are inhibited from propagating. Meanwhile, waves with phase speed in the opposite direction to the mean flow (e.g. Kelvin waves) are free to propagate through the stratosphere until they dissipate or encounter a critical level, depositing their momentum. After sufficient momentum deposition forces the background winds to reverse direction (e.g. from easterly to westerly), the waves that forced the new wind state (e.g. Kelvin waves) are no longer able to propagate, allowing the other regime of waves (e.g. Rossby waves) to propagate and force the zonal wind back to the initial direction (e.g. from westerly to easterly). See Baldwin et al. (2001) for a thorough review of QBO theory and impacts.

A missing component from our understanding of the interaction between Kelvin waves and the QBO is a precise measure of the actual vertical transport of vertical momentum. This transport quantity is most typically written as the eddy vertical momentum flux $\rho\overline{u'w'}$, the density-weighted zonal mean of the product between zonal mean deviations of zonal wind u and vertical wind w. In principle, quantification of this flux only requires knowledge of the zonal distribution of these two fields. Measuring zonal wind does not present any considerable challenges as it has both characteristic speeds that are well above instrument sensitivity and large zonal coherence. Vertical wind, in contrast, does not display either of these advantages: characteristic vertical wind speeds are on the order of 1 cm s^{-1} and zonal variations are large. While some observational platforms – such as flux towers – may reasonably estimate the vertical winds, they are spatially inhomogeneously distributed and only measure within the boundary layer.

Observational shortcomings such as these do not prevent estimation of the Kelvin wave momentum fluxes, however. Maruyama (1968), through judicious application of dynamical theory, showed that the covariance of zonal wind and vertical wind may be approximated by the quadrature spectrum of zonal wind and temperature. That is, the out-of-phase relationship between two readily observable fields – zonal wind and temperature – may be used to estimate the vertical momentum fluxes by Kelvin waves. Later studies based on radiosonde data showed that these waves account for a non-negligible portion of the westerly momentum when the QBO is in its easterly phase (e.g. Sato et al., 1994; Maruyama, 1994). Other theory-based estimates of momentum fluxes have been derived for use with satellite irradiances (Hitchman and Leovy, 1988; Ern and Preusse, 2009) and have found similar magnitudes of the momentum fluxes. Together with estimations using reanalysis products (e.g. Tindall et al., 2006), qualitatively consistent bounds to the momentum flux amplitudes have been determined.

Atmos. Chem. Phys. Discuss., doi:10.5194/acp-2016-1088, 2017
Manuscript under review for journal Atmos. Chem. Phys.
Published: 13 January 2017

Atmospheric Chemistry and Physics Discussions

Yet there remain places where our understanding and estimation may be improved. For instance, few climatological analyses of Kelvin wave momentum fluxes have been performed. While satellite and reanalysis studies have long data records over which to analyze, the vertical resolution of both data sources is greater than a kilometer in the lower stratosphere. It is not clear how sensitive momentum flux calculations are to vertical resolution, particularly for lower stratospheric Kelvin waves with vertical wavelengths on the order of 2-4 km. Kim and Chun (2015) show that such waves may be significantly under-resolved in reanalyses. Studies using high vertical resolution radiosonde data meanwhile only analyzed broad characteristics of Kelvin waves during easterly and westerly QBO phases (e.g. Sato and Dunkerton, 1997), or point estimations of the flux amplitudes (e.g. Holton et al., 2001).

Here we extend previous methods using radiosonde data to analyze climatologies and vertical resolution dependence of Kelvin wave momentum fluxes. We make use of both quality-controlled, high resolution data from a recent field campaign and raw data from long-term radiosonde stations. We apply an algorithm for producing continuous time series of momentum flux estimates. By varying the vertical stepping of input data to the algorithm, we determine the role of vertical resolution on estimations of the fluxes. We then analyze the annual cycle and QBO cycle of these time series of momentum fluxes, demonstrating that our methodology reproduces expected qualitative structures.

Section 2 describes the data and methods we use to generate our flux estimates. Vertical resolution dependence is discussed in Section 3. We present time series of our results in Section 4. Two climatologies are discussed in Section 5. We finish by summarizing and discussing our findings in Section 6.

2 Data and methods

2.1 Data

We primarily use radiosonde data from two sources. The first source contains short-term but high resolution data from the Dynamics of the Madden-Julian Oscillation (DYNAMO) field campaign (Yoneyama et al., 2013). One objective of DYNAMO was to analyze initiation of the Madden-Julian Oscillation (MJO), in part through collection of frequent high-resolution radiosonde data. We use Level 4 radiosonde data (see Ciesielski et al., 2014) from the Gan Island (0.7°S, 73.2°E) and Manus Island (2.0°S, 147.4°E) sounding sites. These Level 4 data are produced at 50 m vertical resolution and 3-hourly temporal resolution. The Gan Island data span from 22 September 2011 to 08 February 2012, while the Manus Island data span from 24 September 2011 to 30 March 2012.

The second source contains lower temporal resolution but longer spanning data from two U.S. Department of Energy Atmospheric Radiation Measurment (ARM) program sounding sites: Manus Island and Nauru Island (0.5°S, 166.9°E). See Mather and Voyles (2013) for a review of ARM facility instruments and missions. Data are recorded every 2 seconds by the sounding packages on launches with frequency ranging from once daily early in the data record to 8 times daily during intensive operation periods such as DYNAMO. The number of data early within the record are insufficient for the spectral filtering we apply so we only consider data from 2003 January 01 to 2013 December 31 for this study. Sondes were launched at least twice daily during this 11 year range.

Atmos. Chem. Phys. Discuss., doi:10.5194/acp-2016-1088, 2017
Manuscript under review for journal Atmos. Chem. Phys.
Published: 13 January 2017

Atmospheric Chemistry and Physics Discussions

Data from the European Centre for Medium Range Weather Forecasting (ECMWF) Interim Reanalysis (ERAi) are also used (Dee et al., 2011) for estimating momentum fluxes and for zonal mean zonal winds. The data are on a regular 0.75° grid in longitude and latitude, and are given at six-hourly temporal resolution. Model level data are used here to take advantage of the highest available vertical resolution in the TTL (∼1000-1500 m).

For composites about the Madden-Julian Oscillation (MJO), we use both the Real-time Multivariate MJO (RMM) index (Wheeler and Hendon, 2004) and the OLR-based MJO (OMI) index (Kiladis et al., 2014). Both indices are based on the principal component time series of the first two empircal orthogonal functions of their input atmospheric fields. For the RMM index, these atmospheric fields are outgoing longwave radiation (OLR) and zonal winds at both 850 hPa and 200 hPa. For the OMI, the only atmospheric field is OLR. As we are most interested here in the generation of Kelvin wave momentum fluxes by convection, we only show MJO composite results using OMI. MJO composites using the RMM index are not qualitatively different.

2.2 Methods

To standardize the vertical and temporal resolutions of the data we use, raw data are linearly interpolated in height and spline interpolated in time. To constrain the interpolation, we require that each output data point have at least 3 input data points within the span from 3 days prior to 3 days following, and at least 3 input data points within the span from 500 m above to 500 m below. Note that this interpolation does not fill all gaps, allowing for missing data to remain. The results are not significantly different for other combinations of linear and spline interpolation, nor for changes to the time range or spatial range in which data points must exist to interpolate to a specified output point. An exception to this is if the time range or spatial range is too small (shorter than 1 day or less than 100 m, respectively) – in this case few output points will be produced.

We range the output temporal resolution Δt_{win} from 6 hours to 48 hours, and the output vertical resolution Δz_{win} from 50 m to 2000 m. These ranges are used to study resolution effects on the calculated momentum fluxes. For our standard analysis, we show temporal resolution of 24 hours and vertical resolution of 250 m. Motivation for why we use these values is given in the next section.

To estimate the Kelvin wave momentum fluxes, we follow the technique described in Sato and Dunkerton (1997) and Holton et al. (2001). Wave solutions to the linearized equatorial beta-plane equations result in

$$\rho\overline{u'w'} = -\rho\frac{R\omega_d}{HN^2}Q_{uT}\,, \tag{1}$$

where R is the gas constant; H is the scale height of the atmosphere, taken to be 7 km here[1]; N^2 is the squared Brunt-Väisälä frequency; Q_{uT} is the quadrature spectrum between u and T, given in units of K m s^{-1}; and ω_d is the intrinsic frequency. Inclusion of density in Eq. (1) casts the momentum flux as a stress term (in units of mPa) from which the vertical gradient approximates the Transformed Eulerian Mean wind forcing

$$\partial_t\overline{u} \propto -\rho^{-1}\partial_z\left(\rho\overline{u'w'}\right)\,. \tag{2}$$

[1]Although this scale height is too short for the lower stratosphere, it is value used in the literature (e.g. Andrews et al., 1987). Hence, we use 7 km to be consistent with past studies.

Atmos. Chem. Phys. Discuss., doi:10.5194/acp-2016-1088, 2017
Manuscript under review for journal Atmos. Chem. Phys.
Published: 13 January 2017

Atmospheric Chemistry and Physics Discussions

Following Andrews et al. (1987), with no meridional wind perturbations v' and the WKB assumption, the intrinsic frequency takes the form

$$\omega_d \equiv \omega - k\overline{u} = -\frac{kN}{m}\,. \tag{3}$$

Here, k is the zonal wavenumber satisfying $k = 2\pi/L_x$, where L_x is the zonal wavelength of the Kelvin waves. m is the vertical wavenumber and is defined to be negative. In deriving the intrinsic frequency, we assume that both the zonal mean zonal wind and stratification N^2 vary in the vertical, but that variations in the stratification are small relative to the vertical wavelength of the waves L_z. This latter assumption is true above the tropopause inversion layer (TIL, e.g. Grise et al., 2010), and we find that 18 km typically lies above the TIL. We thus set the lower boundary of our analysis to this level. For the upper boundary of our analyses, 30 km is a natural choice as few radiosondes reach or extend beyond this level. To highlight results in the lowermost statosphere, we use 25 km as an upper boundary for the presented figures.

The values of ω, i.e. the frequencies relative to the ground, are determined by the frequency bands of the spectral transform we apply to the sounding data. These bands are determined by the time stepping of our data and by the windowing of our spectral decomposition – here taken to be 40 days. This window length allows us to calculate the momentum fluxes at the principal Kelvin wave periods that lie between 5 and 20 days. For the 40 day windowing, the central periods are 20, 13.3, 10, 8, 6.7, 5.7 and 5 days.

The zonal means of zonal wind and temperature are approximated by their time mean over each window. Such an approximation is reasonable in the stratosphere. We have compared our estimates of the zonal mean fields to those calculated from ERAi and found that the fields do not qualitatively differ. From our approximations of $\overline{u}$ and $\overline{T}$, we calculate the zonal deviation fields u' and T', and the stratification N^2.

Vertical wavenumbers m are estimated by modifying a method described in Holton et al. (2001). For each data window, we filter u' and T' for each frequency band using a Butterworth bandpass filter. Then for each of the 40 days within each data window, we find the longest vertically contiguous span of data between 15 and 30 km for both fields at all temporal frequencies. 15 km is used as it represents the upper boundary of convection (e.g., Feng et al., 2014; Xu and Rutledge, 2015) from which Kelvin waves will emanate. The vertical quadrature spectrum $Q_{uT,v}$ is calculated from these contiguous spans of data. From the vertical wavelengths that have phasing such that temperature leads zonal wind, we select the wavelength with the largest negative value of $Q_{uT,v}$. This results in an estimate of L_z for each of the 40 days in a given data window and for each temporal frequency band. We use the window-mean L_z to then calculate the vertical wavenumber $m = 2\pi/L_z$.

This method of estimating the vertical wavenumber was applied to the Nauru99 data that Holton et al. (2001) analyzed. Their estimate of 4.5 km for wave periods of 9-11 days is nearly the same as ours of 4.0 km for the same periods. Likewise, our estimated range of 3.2-5.1 km vertical wavelength for periods of 4-6 days is very similar to the range of 3-4.5 km estimate by Holton et al. (2001).

By finding m, we have all terms in Eq. (3) except the zonal wavenumber k, which can be obtained from the dispersion relation:

$$k = 2\pi/L_x = \omega/\left(\overline{u} - \frac{N}{m}\right)\,. \tag{4}$$

Atmos. Chem. Phys. Discuss., doi:10.5194/acp-2016-1088, 2017
Manuscript under review for journal Atmos. Chem. Phys.
Published: 13 January 2017

Atmospheric Chemistry and Physics Discussions

To ensure that we analyze Kelvin waves, we impose contraints on where the estimated k – and thus momentum flux – are valid. We require that the intrinsic zonal phase speed $\omega_d/k > 0$. We further constrain our analyses to wavelengths greater than 100 km, which captures the observed dominant horizontal Kelvin wave scales of ∼1000 km or larger. Taken together, these constraints require that $k > 0$.

The requirement of positive zonal wavenumber impacts our calculated momentum fluxes because, from Eq. (4), regions of strong easterlies (e.g. where $\overline{u} <$ -20 m s^{-1}) often result in negative k. Because our method assumes that there is a constant vertical wavenumber for a given window of data, it is not able to properly estimate the changes in zonal wavenumber with height, particularly where the zonal wind varies a lot.

Anywhere the above constraints are violated, we set the momentum fluxes to be missing. In order to restrict the impact of these eliminated regions on the analysis presented below, we only retain those points for which every frequency band has real data. This is perhaps more restrictive than is necessary, but ensures consistency, particularly for climatological analyses.

An additional constraint we could apply is that the meridional wind perturbations v' be negligible. This is an important distinguishing property between Kelvin waves and inertio-gravity waves. Appropriately implementing this constraint here is imprecise, however. Unlike with zonal wind, the assumption that the time mean approximates the zonal mean of meridional wind is not accurate. Our estimates of v' will not then be representative of wave perturbations from the zonal mean. Nevertheless, we have tested only retaining data points that fulfill $|v'| < 5$ m s^{-1} and found that our results are not significantly altered by that. Hence, we refrain from applying this constraint.

With all inputs known for Eq. (1), we calculate the momentum flux for each temporal frequency band between 5 and 20 days. Our method of calculation is performed at consecutive windows spaced Δt_{win} apart. We then concatenate all these data windows to produce a time series of total Kelvin wave momentum fluxes. For this time series, the dates of the momentum fluxes we calculate is set to the middle date of each window.

2.3 Example

An example of our method of calculation is shown in Fig. 1. The data for this example are from Gan Island and cover the 40 day window between 21 December 2011 and 29 January 2012. Unfiltered temperature anomalies (shading) and zonal wind anomalies (contours) are shown in panel (a). The signature of Kelvin waves is present here: temperature anomalies lead zonal wind anomalies of the same sign with a roughly 90° phase difference. To better highlight this, panel (b) shows 16-27 day (20 day central period) filtered temperature and zonal wind. From these filtered anomalies, we expect to find large Kelvin wave momentum fluxes in the region between 18 and 21 km.

Atmos. Chem. Phys. Discuss., doi:10.5194/acp-2016-1088, 2017
Manuscript under review for journal Atmos. Chem. Phys.
Published: 13 January 2017

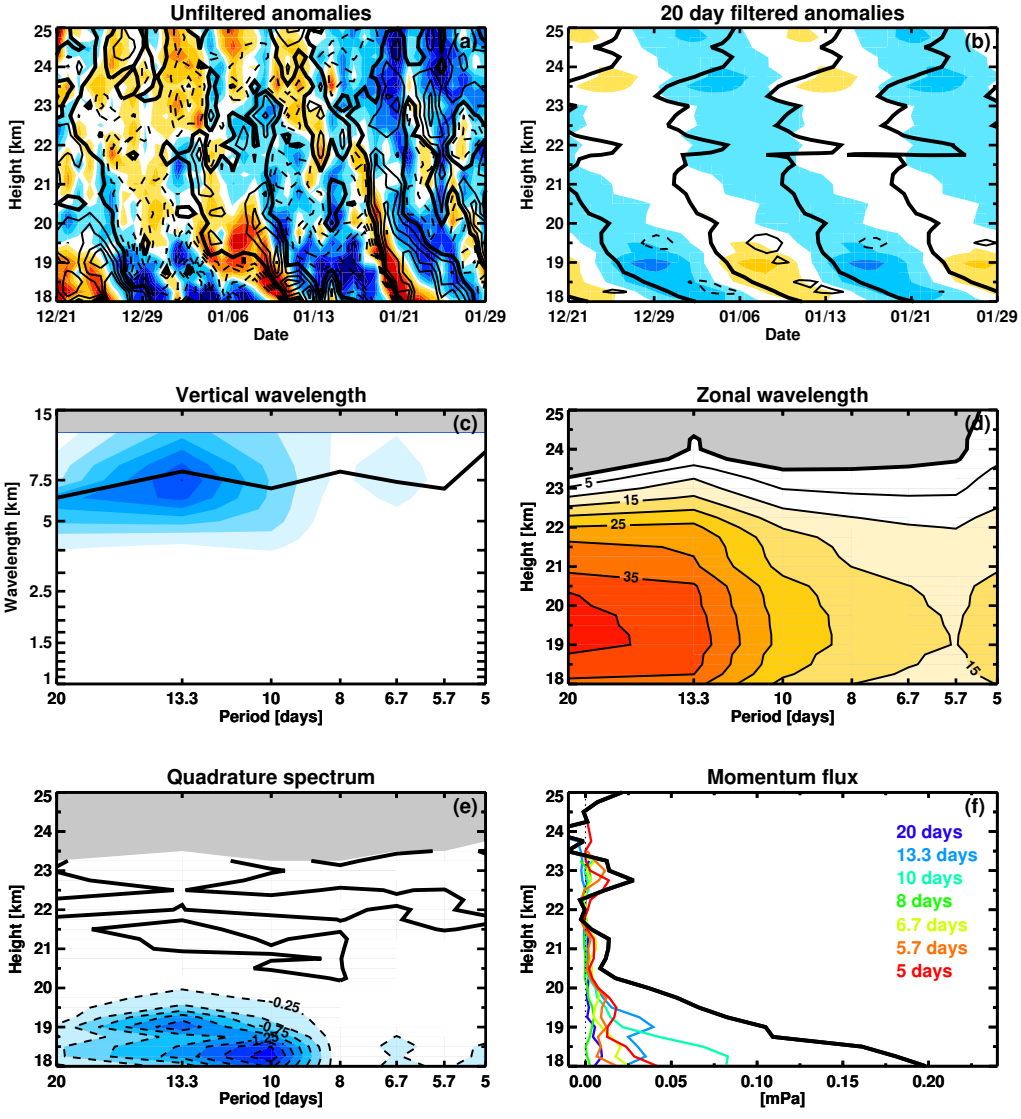

Figure 1. An example of the Kelvin wave momentum flux calculation for Gan Island over the 40 day window between 21 December 2011 and 29 January 2012. (a) Unfiltered zonal temperature anomalies (shading) and zonal wind anomalies (contours). The zonal wind and temperature contour intervals are 3 m s^{-1} and 1 K, respectively. (b) 16-27 day bandpass filtered temperature and zonal wind over the data window. These correspond to the 20 day period waves in our calculations. (c) Vertical quadrature spectrum between u′ and T′ (shading) as a function of period and vertical wavelength and calculated vertical wavelength (black curve, units km) as functions of filtering window. Dark blue shading indicates large magnitudes of the quadrature spectrum. (d) Zonal wavelength as a function of height and of filtering window. Units are 1000 km. (e) The temporal quadrature spectrum between u′ and T′. Units are K m s^{-1}. (f) The calculated total 5-20 day momentum flux (black curve) as a function of height. The colored curves show the contributions from individual filtering windows.

Atmos. Chem. Phys. Discuss., doi:10.5194/acp-2016-1088, 2017
Manuscript under review for journal Atmos. Chem. Phys.
Published: 13 January 2017

Atmospheric Chemistry and Physics Discussions

Panel (c) shows in shading the mean vertical quadrature spectrum as a function of vertical wavelength and frequency. The associated estimate of the vertical wavelengths is overplotted by the black curve. For this window, the waves we analyze have vertical wavelengths between 5-10 km, which fall well within typical observed ranges of vertical wavelengths of equatorial Kelvin waves (e.g., Randel and Wu, 2005).

Zonal wavelengths are shown in (d) as a function of height and of wave period. The longest waves are at the longest periods and primarily below 21 km, as expected from visual inspection of (a). Above ∼23.5 km, the wavelengths are negative for all periods other than 5 days. Since negative L_x is not consistent with the theory used here, we exclude any such regions (gray shading).

Panel (e) shows the quadrature spectrum between zonal wind anomalies and temperature anomalies as a function of period and of height. These spectra are used for calculation of the momentum fluxes shown in panel (f). As expected, the total momentum flux is large between 18 and 20.5 km with a roughly linear decrease in magnitude throughout this vertical span. Above this, the momentum flux is nearly constant with only slight variations up to 25 km. The calculated fluxes in (f) are assigned to 09 January 2012, the central date of the window. Note that the wavenumbers and frequencies derived from the results shown in Fig. 1 are consistent with Kelvin waves (cf. Fig. 3 of Wheeler and Kiladis, 1999).

3 Resolution dependence

We test the dependence of the calculated momentum flux amplitudes on the resolution of input data by independently varying the vertical and temporal resolutions of the imposed interpolation. These tests are performed for a reference level of 18 km. We carry out the following tests at levels above 18 km and find that the results qualitatively hold. At higher levels, a number of complicating effects may come into play. First, coexistence of strong easterlies and relatively short vertical wavelengths occur frequently above 20 km. As discussed in the previous section, such regions violate the assumptions that allow the derivation and application of Eqs. (1) and (3). Second, with increasing height, data gaps are increasingly likely as balloon bursts limit the maximum height of radiosondes. By analyzing just above the tropopause, we are more likely to minimize the impacts from these complications.

To consistently compare the effects of changing vertical and temporal resolutions, we first take the time mean of each of the input fields to Eqs. (1) and (3). Doing so underestimates the true time mean of the momentum fluxes by an average error of ∼3%, but allows us to test which inputs most strongly change the calculated fluxes as either the vertical or temporal resolution is changed. We also only use those data points that are not missing in any of the tested resolutions (total of 377 points).

Fig. 2 (a) shows, as a function of vertical resolution, the mean 5-20 day Kelvin wave momentum fluxes over these common points (solid black). Values of the momentum flux are given on the right axis while percent differences from the reference calculation using 250 m vertical resolution are given on the left axis. There is a strong linear relationship between the vertical resolution and the percent differences of the calculated momentum fluxes, with a mean increase of 1.4% difference for every 100 m increase in vertical stepping.

Atmos. Chem. Phys. Discuss., doi:10.5194/acp-2016-1088, 2017
Manuscript under review for journal Atmos. Chem. Phys.
Published: 13 January 2017

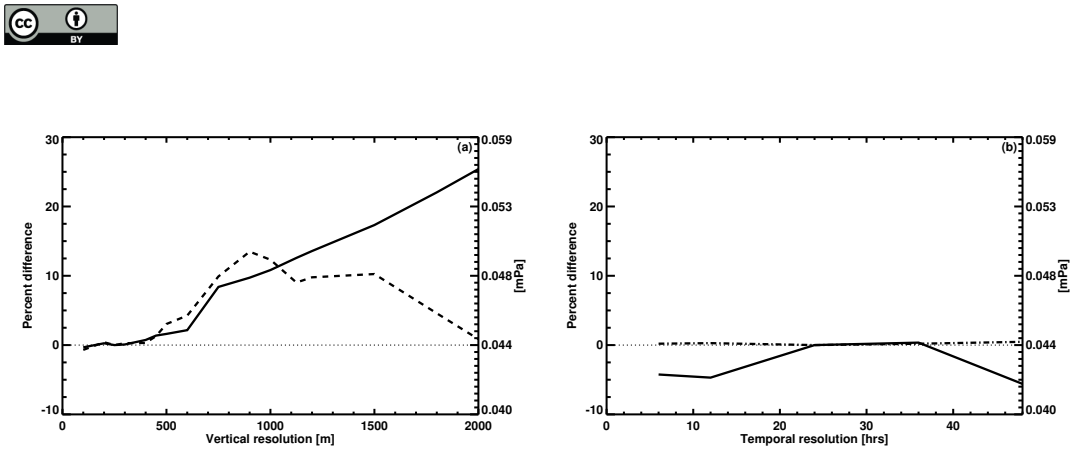

Figure 2. (a) Percent difference in time mean momentum fluxes from 250 m vertical resolution (solid). The right axis gives the values of the mean. The dashed curve shows values for calculations done with L_z set to the 250 m resolution values. (b) Percent difference from 24 hour temporal resolution (solid). The dash-dot curve shows values for calculations done with Q_{uT} set to the 250 m resolution values.

We also study the impact of holding individual input parameters constant at the 250 m resolution value and repeated the calculation. The inputs considered here are stratification N^2, horizontal length scale L_x, vertical length scale L_z, and quadrature spectrum Q_{uT}. Holding N^2, L_x, or Q_{uT} steady is found to not strongly influence the calculated fluxes: the momentum fluxes still increase for increasing vertical resolution at roughly the same rate (not shown).

In contrast, for constant vertical wavelength (dashed), the calculated fluxes increase to 900 m resolution and then decrease for still larger vertical stepping. This suggests that a large portion of the dependence of momentum fluxes on vertical resolution results from changes in the vertical wavelength. To demonstrate how strong this dependence is, the dashed curve shows the mean fluxes if all inputs except the vertical wavelength are held constant at the 250 m value. Up to 900 m resolution, there is little dependence on vertical resolution. Beyond, the fluxes increase rapidly, reaching the same values at 2000 m as those for which all inputs are allowed to vary.

Fig. 2 (b) shows the results from a similar analysis performed for changing temporal resolution. For changes in time stepping, the quadrature spectrum Q_{uT} has the strongest influence on the calculated momentum fluxes. By holding it steady at the 24 hour value (dash-dot), the fluxes remain nearly steady across a range of time resolutions. The primary result here, however, is that the overall variations in calculated momentum fluxes from changes in temporal resolution are much smaller than those from changes in vertical resolution.

4 Time series results

Fig. 3 shows time series of 5-20 day Kelvin wave momentum fluxes calculated from DYNAMO data collected at Gan Island (top) and Manus Island (bottom). Both time series capture the same qualitative structure: enhanced fluxes in October and November 2011, followed by a large, sustained burst that begins in early January 2012. The vertical extents of these momentum fluxes in both time series are also comparable, with amplitudes in both cases negligible above $\sim$21 km. This agreement is

Atmos. Chem. Phys. Discuss., doi:10.5194/acp-2016-1088, 2017
Manuscript under review for journal Atmos. Chem. Phys.
Published: 13 January 2017

Atmospheric Chemistry and Physics Discussions

verified through linear correlation coefficients between the two time series that are between 0.67 and 0.91 at all levels from 18 through 20 km. Lagged correlations do not suggest that there is a time offset between the two time series.

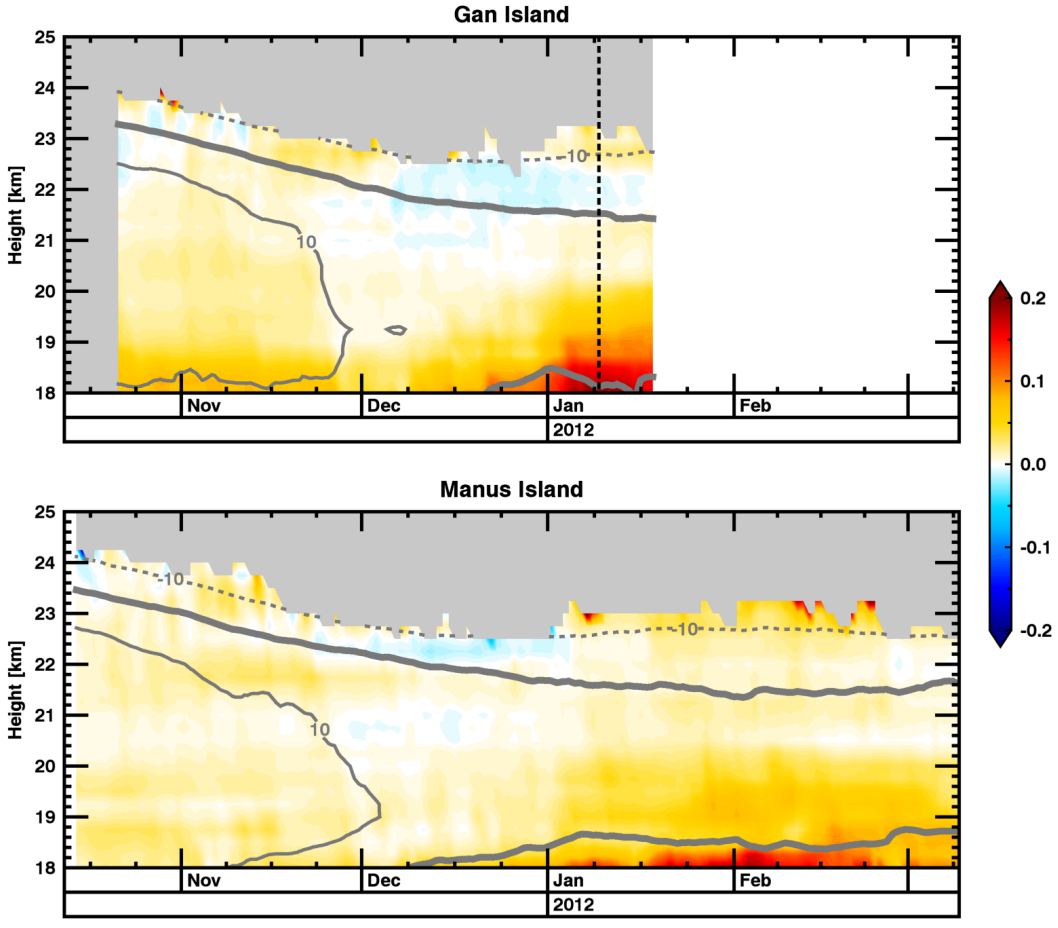

Figure 3. Time series of 5-20 day Kelvin wave momentum fluxes (shading) for Gan Island (top) and Manus Island (bottom) over the DYNAMO field campaign. The dark gray contours give the estimated zonal mean zonal wind at each site; solid contours are westerlies while dashed contours are easterlies. The vertical black dashed line denotes the central date of the window used in Fig. 1. Gray shading indicates where the momentum flux is not being calculated for any frequency band. Momentum flux is in units of mPa and zonal wind contour spacing is 10 m s^{-1}.

A noteworthy difference between the two is that the amplitudes at Gan Island are roughly 2-3 times larger than those at Manus Island. While this is certainly the case for the month of January, it is perhaps more obvious for the period between mid-October and mid-November. This amplitude difference arises in part because our method estimates the full zonal mean momentum fluxes from a point source of data. While Gan Island is located in a region of the Indian Ocean that is relatively far

Atmos. Chem. Phys. Discuss., doi:10.5194/acp-2016-1088, 2017
Manuscript under review for journal Atmos. Chem. Phys.
Published: 13 January 2017

Atmospheric Chemistry and Physics Discussions

removed from other land surfaces, Manus island is located just to the east of the Maritime Continent. The Maritime Continent is known to diminish both Kelvin waves (Flannaghan and Fueglistaler, 2012) and convective signals, such as the MJO (Zhang, 2005), that force these waves.

Figs. 4 and 5 show the time series of momentum fluxes for the Manus ARM site. We find that there is strong qualitative and quantiative agreement between momentum fluxes calculated from both the Manus and Naura ARM sites. See supplementary Figs. S1 and S2 for the time series of momentum fluxes from the Nauru ARM site.

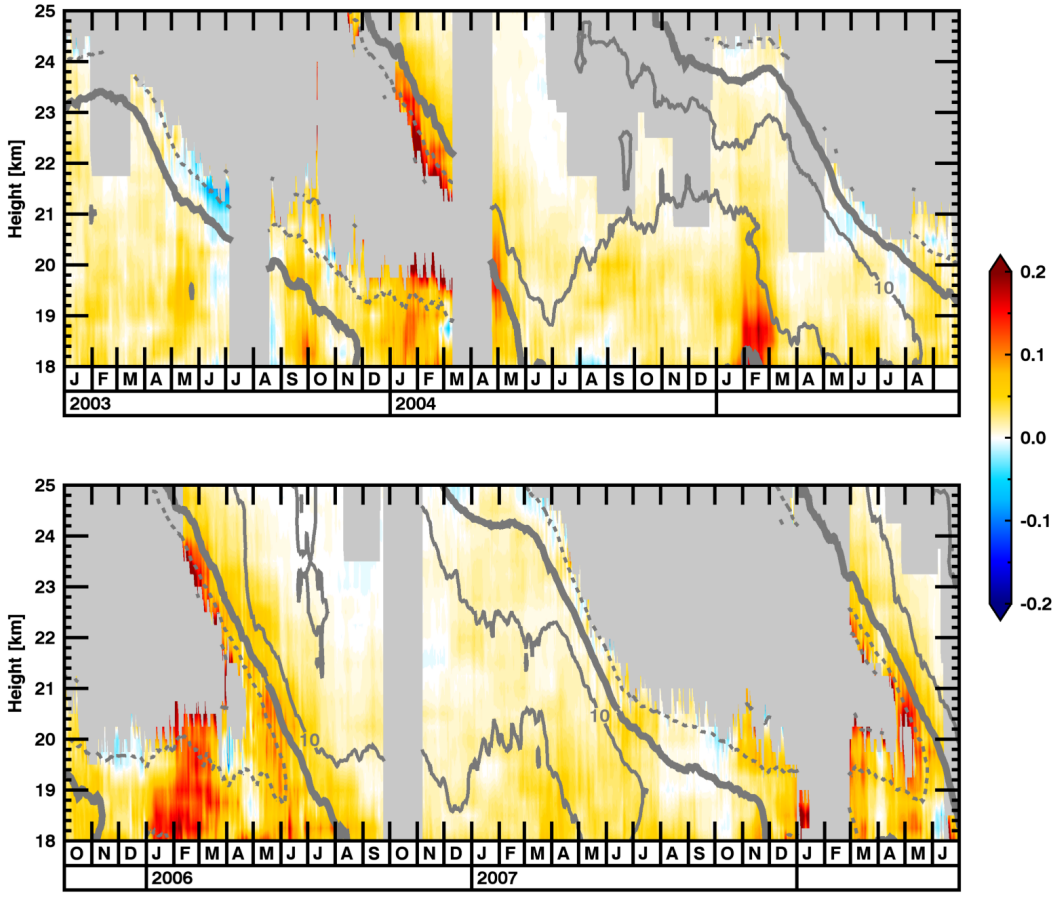

Figure 4. Time series of momentum fluxes from the Manus ARM site. Plotted fields are as in Fig. 3. The span here covers 01 January 2003 through 30 June 2008. Momentum flux is in units of mPa and zonal wind contour spacing (gray contours) is 10 m s^{-1}.

Atmos. Chem. Phys. Discuss., doi:10.5194/acp-2016-1088, 2017
Manuscript under review for journal Atmos. Chem. Phys.
Published: 13 January 2017

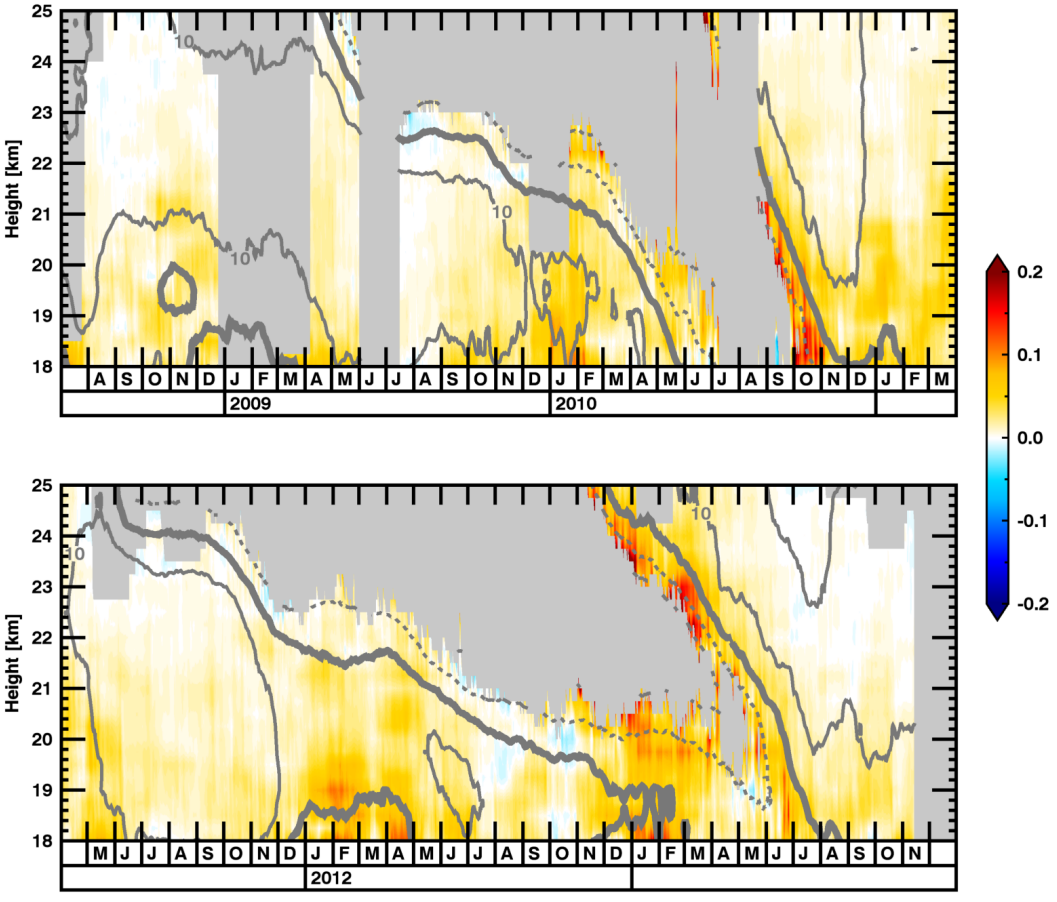

Figure 5. Time series of momentum fluxes from the Manus ARM site, continued. The span here covers 01 July 2008 through 31 December 2013.

In the time series, there are broad regions of data in the center of the easterlies in which the theoretical assumptions are violated (gray shading, see discussion in Section 2); these regions are excluded. Outside of the exclusions, the qualitative patterns of the fluxes match expectations: Kelvin waves are influencing the descent of the westerlies by fluxing westerly momentum there. This is most clearly seen through descending maxima of the flux amplitudes that track the 0 m s^{-1} contour. In westerly QBO phases, these fluxes are nonzero but much smaller.

We find that our estimated momentum flux amplitudes qualitatively agree with those estimated by Ern and Preusse (2009, their Figs. 4 and 5), though with somewhat smaller amplitudes. For example, the momentum flux increase between 18-20 km for JFM in 2006 (bottom panel of Fig. 4) is identified in Ern and Preusse (2009), but their amplitude reaches at least 0.3

Atmos. Chem. Phys. Discuss., doi:10.5194/acp-2016-1088, 2017
Manuscript under review for journal Atmos. Chem. Phys.
Published: 13 January 2017

Atmospheric Chemistry and Physics Discussions

mPa while ours is at most 0.25 mPa. A similar comparison with momentum fluxes derived from ERAi (not shown) also finds qualitative agreement with our amplitudes being smaller.

Calculated momentum fluxes for the Manus ARM site are remarkably similar to those from the Manus DYNAMO data, when the resolution between the two datasets is the same (cf. Fig.3 and the lower panel of Fig. 5). Fidelity between momentum fluxes from both data sources is advantageous to us, as the long record length of the ARM data greatly increases the time over which we can analyze the waves.

5 Annual cycle and QBO

Manus Island climatological annual cycle of momentum fluxes and of input fields to the calculation of Eq. (1) are shown in Fig. 6. These climatologies are smoothed with a 21-day boxcar window for ease of viewing. Panel (a) shows that the lower stratospheric momentum fluxes maximize in January through March (JFM). Each of the input fields to Eq. 1 shows variations that reinforce the variations in momentum flux (panels b-d). Particularly in JFM, the zonal wavelengths become shorter, and the quadrature spectrum amplitude maximizes.

Atmos. Chem. Phys. Discuss., doi:10.5194/acp-2016-1088, 2017
Manuscript under review for journal Atmos. Chem. Phys.
Published: 13 January 2017

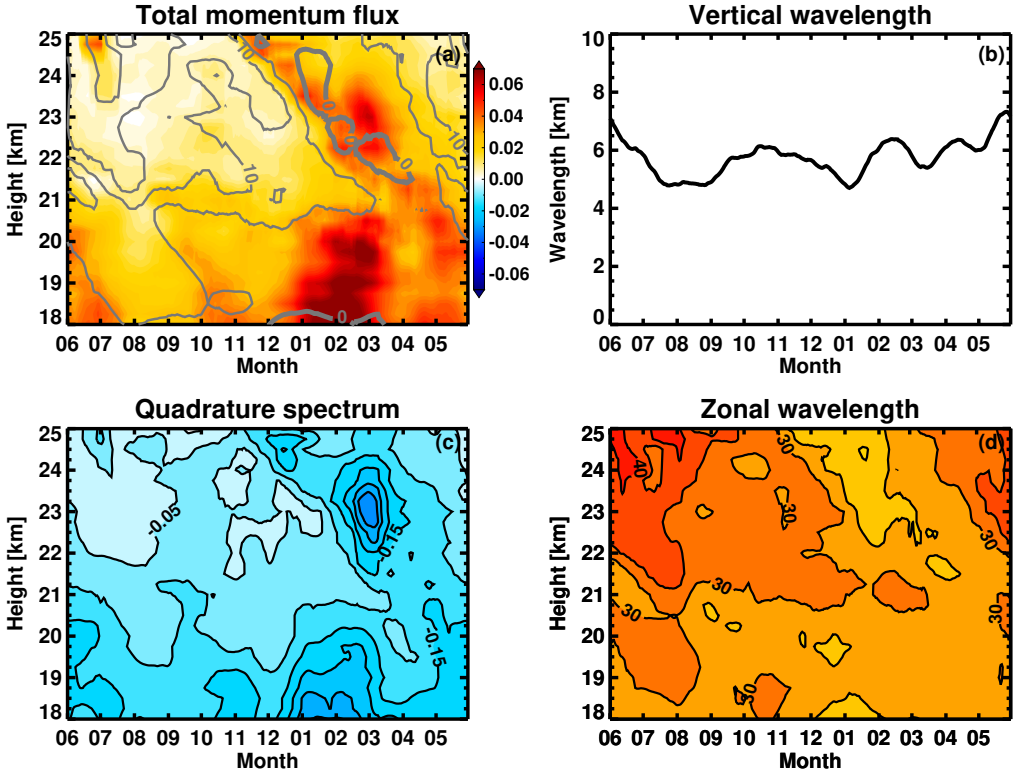

Figure 6. Climatology of momentum flux and related fields from the Manus ARM sounding site. (a) The 5-20 day total momentum flux [mPa] in shading and zonal mean zonal wind in contours. Note that the momentum flux scale is three-tenths of that in Figs. 3 and 4. (b) The vertical length scale L_z [km]. (c) The quadrature spectrum Q_{uT} [K m s^{-1}]. (d) The horizontal length scale L_x [1000 km]. The vertical wavelength, quadrature spectrum, and zonal wavelength are period-weighted means and all fields are 21-day boxcar smoothed.

Panel (a) additionally shows that, over our data record, the westerly QBO phase persists longer in the lower stratosphere than the easterly QBO phase. The momentum fluxes meanwhile are maximized (minimized) in winds that are more easterly (westerly), as expected. This QBO influence on momentum fluxes may more obviously be seen in Fig. 4 through the downward descending amplitudes that fill the region below the 0 m s^{-1} wind contour. Here we analyze the typical momentum fluxes associated with the QBO.

We determine phases of the QBO based on an index of the phasing between zonal mean zonal wind at 30 hPa (U_{30}) and at 50 hPa (U_{50}). Note that our method is qualitatively similar to, though simpler than, the EOF-based index described in Wallace et al. (1993). This index is calculated as

$$QBO_i = \tan^{-1}\left(\frac{U_{50}}{U_{30}}\right) , \tag{5}$$

Atmos. Chem. Phys. Discuss., doi:10.5194/acp-2016-1088, 2017
Manuscript under review for journal Atmos. Chem. Phys.
Published: 13 January 2017

Atmospheric Chemistry and Physics Discussions

and thus ranges from -1 to +1, increasing in time until it reaches +1 and then restarting at -1. QBO_i values between -1 and 0 broadly signify the transition period from easterlies to westerlies throughout the stratosphere, while values between 0 and +1 broadly signify the westerly to easterly transition. By firstly smoothing the zonal winds at both levels with a 31-day boxcar window, this produces a nearly monotonic, cyclic index of the state of the QBO. For this study, we use zonal wind data from ERAi and we split this index into 8 phases with steps of 0.25.

Fig. 7 shows the composite zonal mean zonal wind about this phasing index in gray contours. This composite structure aptly reproduces the expected zonal wind structure of the QBO. For the given 11 years of data, there are four full cycles ranging in length from ∼23.7 months to ∼33.2 months, with a mean length of ∼26.9 months. The range and mean here are well within the observed values (e.g. Baldwin et al., 2001), indicating that this is an appropriate index onto which to composite our calculated momentum fluxes.

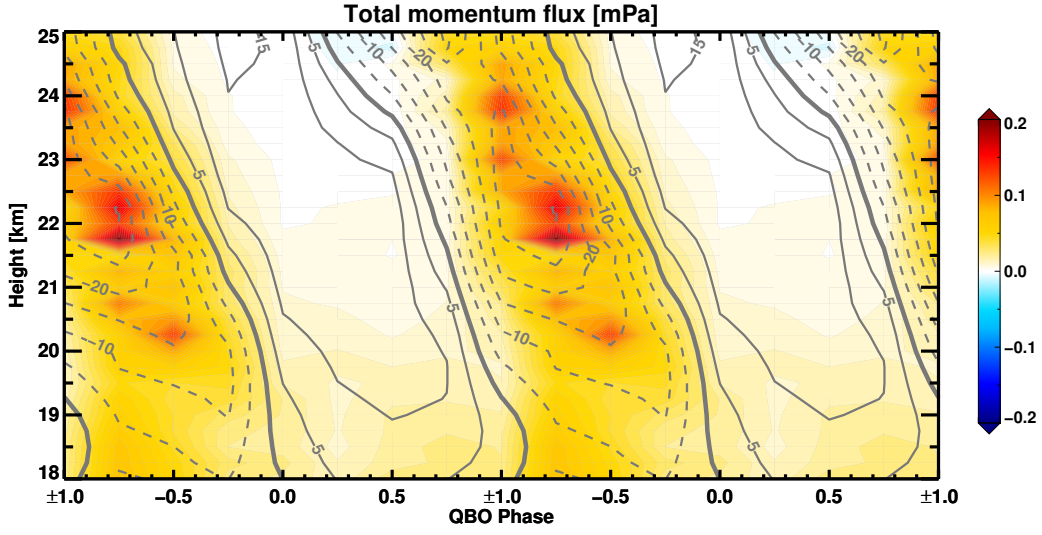

Figure 7. Composite 8-20 day total momentum flux in shading and composite zonal mean zonal winds in gray contours, both as functions of QBO_i (see text for details). Two full cycles of the QBO are shown here to ease visual inspection.

The composite 8-20 day momentum flux fields are also shown in Fig. 7. The 5-20 day composite contains numerous missing data points within the core of the strongest easterlies. These missing data arise from consistently missing data in the 5-8 day period bands for these altitudes and values of QBO_i. The same structure, sans missing data, is captured by the 8-20 day momentum fluxes. Furthermore, the 8-20 day fluxes comprise on average ∼60% of the 5-20 day flux amplitudes during easterly QBO phases. Thus we show the 8-20 day composite for ease of analysis.

The largest Kelvin wave momentum fluxes occur during the transition from easterlies to westerlies, as expected (Holton and Lindzen, 1972). These maxima track downwards with the transition until the lowermost stratospheric wind is westerly. That this descent occurs primarily during DJFM (Fig. 8) explains why the annual mean climatology displays signals of downward

Atmos. Chem. Phys. Discuss., doi:10.5194/acp-2016-1088, 2017
Manuscript under review for journal Atmos. Chem. Phys.
Published: 13 January 2017

descending fluxes during this span. Once the lowermost stratospheric winds are westerly, momentum fluxes become small except within the range of 18-20 km. This is consistent with prior observations of Kelvin waves during westerly QBO phase (Das and Pan, 2013).

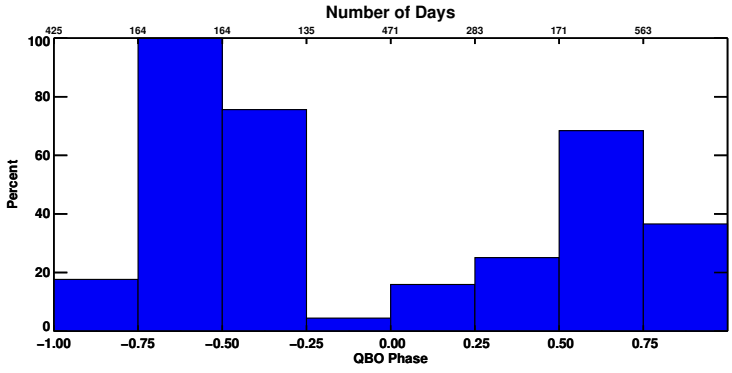

Figure 8. Percent of days in each QBO phase bin that fall between December and March. The total number of days in each bin is given along the top abcissa.

6 Summary and discussion

We expand on prior methods for using high-resolution radiosonde observations to estimate upward fluxes of zonal momentum by Kelvin waves. Our methodology in particular allows for generation of continuous time series of momentum fluxes which are useful for detailed attribution and climatological analyses. The qualitative nature of these time series are found to agree well with previous results – e.g. they show amplification during both JFM and QBO easterly phases – and they qualitatively match prior estimates (cf. Ern and Preusse, 2009, and references therein) though with slightly reduced amplitudes.

Dependence of our results on vertical and temporal resolution is determined by reprocessing raw radiosonde data across different resolutions and comparing spatially and temporally overlapping points from our momentum flux calculation. Temporal resolution does not strongly affect the flux amplitudes for the tested time steps. In contrast, there is an approximately linear increase in the calculated flux amplitudes for linear increases in the vertical resolution, particularly beyond 500 m resolution (Fig. 2). The root of this relationship comes from our method of estimating the vertical wavelength L_z. For lower vertical resolution, less vertical structure is obtained and the calculation tends towards larger estimates of the vertical wavelength. These longer vertical wavelengths result in smaller values of wavenumbers k and m, though the effect on m is larger because it varies proportionally with L_z (cf. Eq. (4)). From Eqs. (1) and (3), it is clear this will result in larger momentum fluxes.

Sensitivity to vertical stepping larger than 500 m highlights the need for continued collection of high vertical resolution observations in the tropical stratosphere. Both satellite observations and reanalysis reconstructions have much larger (order 1 km and larger) vertical stepping at these altitudes, so estimations derived from these sources alone may not fully capture

Atmos. Chem. Phys. Discuss., doi:10.5194/acp-2016-1088, 2017
Manuscript under review for journal Atmos. Chem. Phys.
Published: 13 January 2017

Atmospheric Chemistry and Physics Discussions

the vertical structure. The impact of this may be seen by the larger momentum flux amplitudes derived from these sources. Advances in remote sensing and computing capabilities will allow for smaller vertical stepping in both these platforms, helping to alleviate this sensitivity. However, there will still be a significant role for routine, high resolution radiosonde data in constraining satellite observations and in nudging data assimilation procedures for reanalyses.

By comparing calculated fluxes from highly-processed radiosonde data during the DYNAMO field campaign to calculated fluxes from synchronous raw radiosonde data at identical and nearby sounding stations, we find that our method is well-suited for application to these raw data, of which there is a considerably longer data record. Kelvin wave momentum fluxes are then calculated from an 11 year span (2003-2013) of quality radiosonde observations from this data record. The annual mean cycle of momentum fluxes shows an annual periodicity with a JFM maximum and minimum six months later for July through September (Fig. 6). The QBO mean momentum fluxes are large during easterly phase and small during westerly phase (Fig. 7), as expected.

There is an important interpretation of the above results that arises when comparing simultaneous calculations of momentum fluxes at different sounding sites (see Figs. 3 and 4): our technique for calculating zonal mean momentum fluxes is strongly influenced by the local contribution to the zonal mean. For the DYNAMO data, Gan Island observations occur within the Indian Ocean where strong convection associated with the MJO is common. The expansive convection associated with these MJO events experienced at Gan Island propagates eastward to Manus Island, but is diminished after propagating over the Maritime Continent (Zhang, 2005). One would expect that such a disruption to the convection will lead to a disruption in the generation of Kelvin waves. This may, in part, explain why the estimated momentum flux amplitudes are smaller at Manus Island, located to the east of the Maritime Continent. Fluxes at Nauru, $\sim 20^{\circ}$ to the east of Manus, are similarly smaller (see Figs. S1 and S2).

Our calculated momentum fluxes largely represent local contributions to the zonal mean. However, stratospheric Kelvin waves are known to strongly project onto plantery scales (i.e. zonal wavenumbers 1-3, Feng et al., 2007). This projection may be in part from a quasi-stationary source of these waves: frequent convection over the Indian Ocean and Maritime Continent. It is possible that data from Indian Ocean sounding sites routinely sample the ridges of these planetary-scale, zonal mean momentum fluxes. Our results may then give an upper estimate of the Kelvin wave momentum flux amplitudes. Future, more detailed analyses may reveal more insights into this issue.

A natural step in this line of study is attribution of convective signals to enhanced lower stratospheric Kelvin wave momentum fluxes. We investigated the influence of the MJO, i.e. the dominant intraseasonal pattern in tropical convection, in determining the amplitudes and temporal structure of the derived climatologies.

Atmos. Chem. Phys. Discuss., doi:10.5194/acp-2016-1088, 2017
Manuscript under review for journal Atmos. Chem. Phys.
Published: 13 January 2017

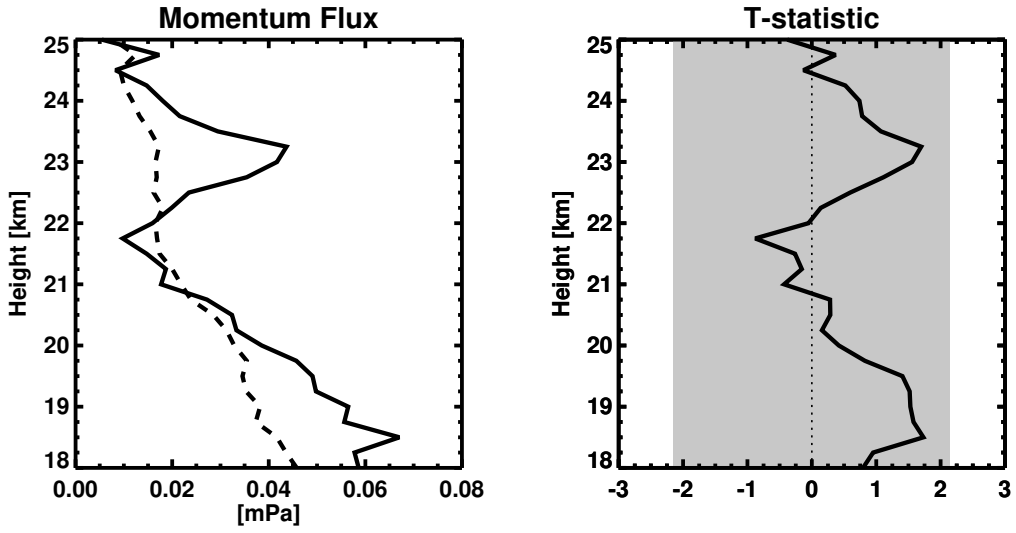

Figure 9. (left) Mean momentum flux during MJO active periods (solid) and the entire data record (dashed). MJO active periods are where OMI index is greater than 1 for at least 40 days (16 total events). (right) T-statistics for the difference of means between MJO active periods and the total record. Values outside of the gray shading are significant at the 95% level.

The left panel of Fig. 9 shows the mean momentum flux for MJO active periods (solid). MJO active periods are typically defined where the OMI amplitude is at least 1. Here, to ensure that our MJO active period composite does not alias data from inactive periods (OMI amplitude < 1), we require that all days in a given data window must have OMI amplitude ≥ 1. While such points are infrequent (15 distinct events in our data record), they are more likely to have a strong wave signal that projects onto our analyzed periods. We then compare this composite to the entire record (dashed) so as to analyze if the MJO is significantly different from the record mean. Using a comparable separation for MJO inactive period – all days in a given window must have OMI amplitude < 1 – results in relatively few data points.

Though the momentum fluxes in the lowermost stratosphere are larger during MJO active periods, they are not statistically significantly different at the 95% level (right panel). Composite momentum fluxes between 18.5 and 19.5 km are significantly different only at the 85% significance level. This lower stratospheric difference between MJO active periods and the mean state is considerably lower at Nauru Island, further lowering confidence in these results. Furthermore, while the 23 km peak approaches the same level of significant difference, it is well removed from the signal in the lowermost stratosphere. This separation from the source region for Kelvin waves indicates that it is a possible spurious difference. That the above differences are not significant is consistent with previous studies, e.g. Virts and Wallace (2014), that show that MJO inactive periods have considerable Kelvin wave activity in the lower stratosphere.

The MJO amplitude is known to have a seasonal cycle that reaches its maximum during DJF (Zhang, 2005), so we analyzed to what degree the MJO affects the JFM maximum of momentum flux (Fig. 6). While the fluxes during MJO active times

Atmos. Chem. Phys. Discuss., doi:10.5194/acp-2016-1088, 2017
Manuscript under review for journal Atmos. Chem. Phys.
Published: 13 January 2017

are larger than those during inactive times (not shown), the differences are not significant at a meaningful significance level. An analogous separation of the QBO composite into MJO active and inactive times (not shown) finds that the lowermost stratospheric momentum fluxes are larger when the MJO is active, though the results are again not statistically significant.

However, finding significance with such a statistical analysis is complicated by both the techniques and data used here. The 40 day windowing we use effectively applies a smoothing on the data that is of the order of the typical MJO periodicity of 30-90 days. Thus zonal wind and temperature data points from both inactive and active times are blended together for some calculated momentum flux data points. As shown by Fig. 9, comparing only those data points that fall within MJO active spans of 40 days or longer with data points that fall completely outside of MJO active spans does not change the significance result.

Doing so in fact only exacerbates an additional complication from the relatively short record length of data. Only 15 events are used in Fig. 9. In our comparison of annual cycles between MJO active and inactive periods, the median number of data points used for each day are seven and four, respectively. For any statistical tests we may apply, the degrees of freedom are small enough that the differences in the composites would need to be dramatic for significance. The differences in QBO composites (not shown) would need to be yet larger since there are only four observed cycles in this data record. Our investigation of MJO influence thus leaves us only with the suggestion of a nontrivial increase in fluxes from enhanced convection during MJO active times, but further study is needed.

Such studies should continue technique developments and data analyses that are necessary to further constrain the tropical stratospheric momentum flux budget. Techniques could be developed to incorporate simultaneous soundings from multiple sites into a single calculation of momentum fluxes. The results derived here come from two radiosonde sites, but many additional sites with long data records are available. A careful reprocessing of these radiosonde data may allow for extending the data record with already available data.

Continued collection of high-quality radiosonde observations that probe the tropical stratosphere will also be vital for increasing the number of observed annual and QBO cycles. In addition to the role radiosondes have in forecasting (e.g. Cardinali and Healy, 2014) and climatological studies (e.g. Seidel et al., 2012), recently observed anomalous evolution of the QBO (Newman et al., 2016) further bears out the need for continued radiosonde observations. Additional observations in this region will allow for more robust attribution of wave sources – whether Kelvin, Rossby, or gravity waves – to changes in zonal wind structure in the tropical stratosphere.

Competing interests. The authors declare that they have no conflict of interest.

Acknowledgements. The authors would like to acknowledge Paul Ciesielski for his help in obtaining the L4 DYNAMO data and the raw radiosonde data.

Atmos. Chem. Phys. Discuss., doi:10.5194/acp-2016-1088, 2017
Manuscript under review for journal Atmos. Chem. Phys.
Published: 13 January 2017

Atmospheric Chemistry and Physics Discussions

References

Andrews, D. G., Holton, J. R., and Leovy, C. B.: Middle Atmosphere Dynamics, Academic Press, 1987.

Baldwin, M. P., Gray, L. J., Dunkerton, T. J., Hamilton, K., Haynes, P. H., Randel, W. J., Holton, J. R., Alexander, M. J., Hirota, I., Horinouchi, T., Jones, D. B. A., Kinnersley, J. S., Marquardt, C., Sato, K., and Takahashi, M.: The quasi-biennial oscillation, Rev. Geophys., 39, 179–229, doi:8755-1209/01/1999RG000073, 2001.

Cardinali, C. and Healy, S.: Impact of GPS radio occultation measurements in the ECMWF system using adjoint-based diagnostics, Q. J. R. Meteorol. Soc., 140, 2315–2320, doi:10.1002/qj.2300, 2014.

Ciesielski, P. E., Yu, H., Johnson, R. H., Yoneyama, K., Katsumata, M., Long, C. N., Wang, J., Loehrer, S. M., Young, K., Williams, S. F., Brown, W., Braun, J., and Van Hove, T.: Quality-controlled upper-air sounding dataset for DYNAMO/CINDY/AMIE: development and corrections, J. Atmos. Oceanic Technol., 31, 741–764, doi:10.1175/JTECH-D-13-00165.1, 2014.

Collimore, C. C., Martin, D. W., Hitchman, M. H., Huesman, A., and Waliser, D. E.: On The relationship between the QBO and tropical deep convection, J. Climate, 16, 2552–2568, doi:10.1175/1520-0442(2003)016<2552:OTRBTQ>2.0.CO;2, 2003.

Das, U. and Pan, C. J.: Strong Kelvin wave activity observed during the westerly phase of QBO – a case study, Ann. Geophys., 31, 581–590, doi:10.5194/angeo-31-581-2013, 2013.

Dee, D. P., Uppala, S. M., Simmons, A. J., Berrisford, P., Poli, P., Kobayashi, S., Andrae, U., Balmaseda, M. A., Balsamo, G., Bauer, P., Bechtold, P., Beljaars, A. C. M., van de Berg, L., Bidlot, J., Bormann, N., Delsol, C., Dragani, R., Fuentes, M., Geer, A. J., Haimberger, L., Healy, S. B., Hersbach, H., Holm, E. V., Isaksen, L., Kallberg, P., Kohler, M., Matricardi, M., McNally, A. P., Morcrette, B. M. M.-S. J.-J., Park, B.-K., Puebey, C., de Rosnay, P., Tavolato, C., Thepaut, J.-N., and Vitart, F.: The ERA-Interim reanalysis: configuration and performance of the data assimiliation system, Q. J. R. Meterol. Soc., 137, 553–597, doi:10.1002/qj.828, 2011.

Ern, M. and Preusse, P.: Wave fluxes of equatorial Kelvin waves and QBO zonal wind forcing derived from SABER and ECMWF temperature space-time spectra, Atmos. Chem. Phys., 9, 3957–3986, doi:10.5194/acp-9-3957-2009, 2009.

Feng, L., Harwood, R. S., Brugge, R., O'Neill, A., Froidevaux, L., Schwartz, M., and Waters, J. W.: Equatorial Kelvin waves as revealed by EOS Microwave Limb Sounder observations and European Centre for Medium-Range Weather Forecasts analyses: evidence for slow Kelvin waves of zonal wave number 3, J. Geophys. Res., 112, D16 106, doi:10.1029/2006JD008329, 2007.

Feng, Z., McFarlane, S. A., Schumacher, C., Ellis, S., Comstock, J., and Bharadwaj, N.: Constructing a merged cloud-precipitation radar dataset for tropical convective clouds during the DYNAMO/AMIE experiment at Addu Atoll, J. Atmos. Oceanic Technol., 31, 1021–1042, doi:10.1175/JTECH-D-13-00132.1, 2014.

Flannaghan, T. J. and Fueglistaler, S.: Tracking Kelvin waves from the equatorial troposphere into the stratosphere, J. Geophys. Res., 117, D21 108, doi:10.1029/2012JD017448, 2012.

Fueglistaler, S. and Haynes, P. H.: Control of interannual and longer-term variability of stratospheric water vapor, J. Geophys. Res., 110, D24 108, doi:10.1029/2005JD006019, 2005.

Garfinkel, C. I., Shaw, T. A., Hartmann, D. L., and Waugh, D. W.: Does the Holton–Tan mechanism explain how the quasi-biennial oscillation modulates the arctic polar vortex?, J. Atmos. Sci., 69, 1713–1733, doi:10.1175/JAS-D-11-0209.1, 2012.

Gill, A. E.: Atmosphere-Ocean Dynamics, Academic Press, 1982.

Grise, K. M., Thompson, D. W. J., and Birner, T.: A global survey of static stability in the stratosphere and upper troposphere, J. Climate, 23, 2275–2292, doi:10.1175/2009JCLI3369.1, 2010.

Hitchman, M. H. and Leovy, C. B.: Estimation of the Kelvin wave contribution to the semiannual osccilation, J. Atmos. Sci., 45, 1462–1475, doi:10.1175/1520-0469(1988)045<1462:EOTKWC>2.0.CO;2, 1988.

Holton, J. R. and Lindzen, R. S.: An updated theory for the quasi-biennial cycle of the tropical stratosphere, J. Atmos. Sci., 29, 1076–1080, doi:10.1175/1520-0469(1972)029<1076:AUTFTQ>2.0.CO;2, 1972.

Holton, J. R., Alexander, M. J., and Boehm, M. T.: Evidence for short vertical wavelength Kelvin waves in the Department of Energy-Atmospheric Radiation Measurement Nauru99 radiosonde data, J. Geophys. Res., 106, 20,125–20,129, doi:10.1029/2001JD900108, 2001.

Kiladis, G. N., Wheeler, M. C., Haertel, P. T., Straub, K. H., and Roundy, P. E.: Convectively coupled equatorial waves, Rev. Geophys., 47, RG2003, doi:10.1029/2008RG000266, 2009.

Kiladis, G. N., Dias, J., Straub, K. H., Wheeler, M. C., Tulich, S. N., Kikuchi, K., Weickmann, K. M., and Ventrice, M. J.: A comparison of OLR and circulation-based indices for tracking the MJO, Mon. Wea. Rev., 142, 1697–1715, doi:10.1175/MWR-D-13-00301.1, 2014.

Kim, Y.-H. and Chun, H.-Y.: Momentum forcing of the quasi-biennial oscillation by equatorial waves in recent reanalyses, Atmos. Chem. Phys., 15, 6577–6587, doi:10.5194/acp-15-6577-2015, 2015.

Maruyama, T.: Upward transport of westerly momentum due to large-scale disturbances in the equatorial lower stratosphere, J. Met. Soc. Japan, 46, 404–417, 1968.

Maruyama, T.: Upward transport of westerly momentum due to disturbances of the equatorial lower stratosphere in the period range of about 2 days – a Singapore data analysis for 1983-1993, J. Met. Soc. Japan, 72, 423–432, 1994.

Mather, J. H. and Voyles, J. W.: The ARM climate research facility, Bull. Amer. Meteor. Soc., 94, 377–392, doi:10.1175/BAMS-D-11-00218.1, 2013.

Newman, P. A., Coy, L., Pawson, S., and Lait, L. R.: The anomalous change in the QBO in 2015–2016, Geophys. Res. Lett., 43, doi:10.1002/2016GL070373, 2016.

Randel, W. J. and Wu, F.: Isolation of the ozone QBO in SAGE II data by singular-value decomposition, J. Atmos. Sci., 53, 2546–2559, doi:10.1175/1520-0469(1996)053<2546:IOTOQI>2.0.CO;2, 1996.

Randel, W. J. and Wu, F.: Kelvin wave variability near the equatorial tropopause observed in GPS radio occulation measurements, J. Geophys. Res., 110, D03 102, doi:10.1029/2004JD005006, 2005.

Sato, K. and Dunkerton, T. J.: Estimates of momentum flux associated with equatorial Kelvin and gravity waves, J. Geophys. Res., 102, 26,247–26,261, doi:10.1029/96JD02514, 1997.

Sato, K., Hasegawa, F., and Hirota, I.: Short-period disturbances in the equatorial lower stratosphere, J. Met. Soc. Japan, 72, 859–872, 1994.

Seidel, D. J., Free, M., and Wang, J. S.: Reexamining the warming in the tropical upper troposphere: models versus radiosonde observations, Geophys. Res. Lett., 39, L22 701, doi:10.1029/2012GL053850, 2012.

Straub, K. H., Kiladis, G. N., and Ciesielski, P. E.: The role of equatorial waves in the onset of the South China Sea summer monsoon and the demise of El Niño during 1998, Dyn. Atmos. Oceans, 42, 216–238, doi:10.1016/j.dynatmoce.2006.02.005, 2006.

Thompson, D. W. J., Baldwin, M. P., and Wallace, J. M.: Stratospheric connection to Northern Hemisphere wintertime weather: implications for prediction, J. Climate, 15, 1421–1428, doi:10.1175/1520-0442(2002)015<1421:SCTNHW>2.0.CO;2, 2002.

Tindall, J. C., Thuburn, J., and Highwood, J.: Equatorial waves in the lower stratosphere. II: annual and interannual variability, Q. J. R. Meteorol. Soc., 132, 195–212, doi:10.1256/qj.04.153, 2006.

Virts, K. S. and Wallace, J. M.: Observations of temperature, wind, cirrus, and trace gases in the tropical tropopause transition layer during the MJO, J. Atmos. Sci., 71, 1143–1157, doi:10.1175/JAS-D-13-0178.1, 2014.

Wallace, J. M., Panetta, R. L., and Estberg, J.: Representation of the equatorial stratospheric quasi-biennial oscillation in EOF phase space, J. Atmos. Sci., 50, 1751–1762, doi:10.1175/1520-0442(1993)006<2063:SASOIA>2.0.CO;2, 1993.

Wheeler, M. and Kiladis, G. N.: Convectively coupled equatorial waves: analysis of clouds and temperature in the wavenumber-frequency domain, J. Atmos. Sci., 56, 374–399, doi:10.1175/1520-0469(1999)056<0374:CCEWAO>2.0.CO;2, 1999.

Wheeler, M. C. and Hendon, H. H.: An all-season real-time multivariate MJO index: development of an index for monitoring and prediction, Mon. Wea. Rev., 132, 1917–1932, doi:10.1175/1520-0493(2004)132<1917:AARMMI>2.0.CO;2, 2004.

Xu, W. and Rutledge, S. A.: Morphology, intensity, and rainfall production of MJO convection: observations from DYNAMO shipborne radar and TRMM, J. Atmos. Sci., 72, 623–640, doi:10.1175/JAS-D-14-0130.1, 2015.

Yoneyama, K., Zhang, C., and Long, C. N.: Tracking pulses of the Madden-Julian Oscillation, Bull. Amer. Soc., 94, 1871–1891, doi:10.1175/BAMS-D-12-00157.1, 2013.

Zhang, C.: Madden-Julian Oscillation, Rev. Geophys., 43, RG2003, doi:10.1029/2004RG000158, 2005.